

An Extragalactic Spectroscopic Survey of the SSA22 Field

C. Saez,¹ B. D. Lehmer,^{2,3} F. E. Bauer,^{4,5,6} D. Stern,⁷ A. Gonzales,⁸ I. Rreza,⁹
 D. M. Alexander,¹⁰ Y. Matsuda,^{11,12} J. E. Geach,¹³ F. A. Harrison⁹ and
 T. Hayashino¹⁴

¹*Department of Astronomy, University of Maryland, College Park, MD 20742-2421, USA*

²*The Johns Hopkins University, Homewood Campus, Baltimore, MD 21218, USA*

³*NASA Goddard Space Flight Center, Code 662, Greenbelt, MD 20771, USA*

⁴*Instituto de Astrofísica, Facultad de Física, Pontificia Universidad Católica de Chile, 306, Santiago 22, Chile*

⁵*Millennium Institute of Astrophysics, Santiago, Chile*

⁶*Space Science Institute, 4750 Walnut Street, Suite 205, Boulder, Colorado 80301*

⁷*Jet Propulsion Laboratory, California Institute of Technology, Pasadena, CA 91109*

⁸*Department of Earth, Atmospheric and Planetary Sciences, Massachusetts Institute of Technology, Cambridge, MA 02139*

⁹*Cahill Center for Astrophysics, California Institute of Technology, Pasadena, CA 91125*

¹⁰*Department of Physics, Durham University, Durham DH1 3LE, UK*

¹¹*National Astronomical Observatory of Japan, 2-21-1 Osawa, Mitaka, Tokyo 181-8588, Japan*

¹²*The Graduate University for Advanced Studies (SOKENDAI), 2-21-1 Osawa, Mitaka, Tokyo 181-0015, Japan*

¹³*Centre for Astrophysics Research, Science & Technology Research Institute, University of Hertfordshire, Hatfield, AL10 9AB, UK*

¹⁴*Astronomical Institute, Tohoku University, Aramaki, Aoba-ku, Sendai, Miyagi, 980-8578, Japan*

ABSTRACT

We present VLT VIMOS, Keck DEIMOS and Keck LRIS multi-object spectra of 367 sources in the field of the $z \approx 3.09$ protocluster SSA22. Sources are spectroscopically classified via template matching, allowing new identifications for 206 extragalactic sources, including 36 $z > 2$ Lyman-break galaxies (LBGs) and Lyman- α emitters (LAEs), 8 protocluster members, and 94 X-ray sources from the ~ 400 ks *Chandra* deep survey of SSA22. Additionally, in the area covered by our study, we have increased by ≈ 4 , 13, and 6 times the number of reliable redshifts of sources at $1.0 < z < 2.0$, at $z > 3.4$, and with X-ray emission, respectively. We compare our results with past spectroscopic surveys of SSA22 to investigate the completeness of the LBGs and the X-ray properties of the new spectroscopically-classified sources in the SSA22 field.

Key words: surveys — techniques: imaging spectroscopy — X-rays: galaxies — galaxies: clusters: general — galaxies: active.

1 INTRODUCTION

The SSA22 field hosts one of the most distant and well studied protoclusters currently known. Originally discovered by Steidel et al. (1998), the SSA22 protocluster lies at $z = 3.09$ and contains several powerful active galactic nuclei (AGNs; Lehmer et al. 2009a,b), numerous Lyman-break galaxies (LBGs; Steidel et al. 1998, 2003) and Lyman- α emitters (LAEs; Hayashino et al. 2004; Matsuda et al. 2005), and multiple spatially extended Lyman- α blobs (Steidel et al. 2000; Matsuda et al. 2004, 2011), the most extreme of which span regions $> 100 h^{-1} \text{kpc}$ in extent. The protocluster has been mapped using the LAE population, which has revealed a belt-like structure across a $60 \times 20 \text{ Mpc}^2$ (comoving size) region (Hayashino et al. 2004; Yamada et al. 2012). At its core, the protocluster reaches a factor of ≈ 6 times overden-

sity of LBGs and LAEs compared to the field (Steidel et al. 2000). Cosmological models predict that the protocluster would have collapsed into a $z = 0$ structure resembling a rich local cluster (e.g., Coma) with a total mass $> 10^{15} M_{\odot}$ (see, e.g., Governato et al. 1998; Steidel et al. 1998).

Since the discovery of the protocluster, the SSA22 field has been extensively studied at several wavelengths, providing new information about how galaxies grow in high density environments at $z \approx 3$ (e.g., Chapman et al. 2001, 2004; Geach et al. 2005; Webb et al. 2009; Nestor et al. 2011; Tamura et al. 2009, 2010, 2013; Uchimoto et al. 2012; Kubo et al. 2013). To address how the supermassive black hole (SMBH) populations in the protocluster environment are growing, a deep ≈ 400 ks *Chandra* survey was conducted over the SSA22 field: the *Chandra* Deep Protocluster Survey

(Lehmer et al. 2009b).¹ The *Chandra* exposure over SSA22 yielded multiple detections for LBGs and LAEs associated with the $z = 3.1$ protocluster. Early results indicated that the fraction of protocluster galaxies hosting AGN was elevated by a factor of $6.1^{+10.3}_{-3.6}$ compared to the field population at $z \approx 3$, suggesting the presence of an enhanced AGN duty cycle and/or more massive SMBHs in the $z \approx 3$ protocluster environment (Lehmer et al. 2009a). Additional AGN studies of clusters and protoclusters have confirmed a steady rise in the AGN fraction for galaxies in the highest density environments with increasing redshift (e.g., Martini et al. 2009, 2013; Digby-North et al. 2010; Lehmer et al. 2013), implying that the key growth phases of the most massive SMBHs occurred in high-redshift protoclusters like that found in SSA22.

Prior to the current work, the *Chandra* SSA22 point source catalog from Lehmer et al. (2009b) contained robust redshift matches for only $\approx 10\%$ of the X-ray sources, limiting initial constraints on the AGN activity in the protocluster to a small subset of sources in the field. Additionally, there is only one published LBG spectroscopic catalog in the SSA22 field (Steidel et al. 2003). This survey only covered the area around the center of the protocluster and yielded spectroscopic measurements for $\approx 50\%$ of the known LBGs. Therefore, in order to better characterize the AGN activity in the SSA22 protocluster it is imperative to unambiguously identify protocluster members by obtaining spectroscopic measurements of both the galaxies (LBGs and LAEs) and X-ray sources in the field.

In this paper, we present a survey of extragalactic sources in the SSA22 field using the multi-object spectrographs at the Very Large Telescope (VLT) and Keck. We map the SSA22 field with the dual goals of identifying new protocluster members and complementing previous studies performed in this field. We target new LBGs in the redshift range of the SSA22 protocluster, as well as X-ray sources detected in the *Chandra* Deep Protocluster Survey. The structure of the paper is as follows: in §2 we outline our observations and the data reduction strategies; in §3 we detail our spectral template matching approach used to identify the sources; in §4 we describe the main results; and in §5 we summarize our work. Throughout this work, unless stated otherwise, the errors listed are at the 1σ level, we use AB magnitudes, CGS units, and adopt the concordance cosmology, $\Omega_M = 0.3$, $\Omega_\Lambda = 0.7$ and $H_0 = 70 \text{ km s}^{-1} \text{ Mpc}^{-1}$.

2 OBSERVATIONS AND DATA REDUCTION

Our observations were conducted using multiple slit mask exposures of the Visible Multi-Object Spectrograph (VIMOS; Le Fèvre et al. 2003) on the VLT, and the Deep Imaging Multi-Object Spectrograph (DEIMOS; Faber et al. 2003) and Low Resolution Imaging Spectrometer (LRIS; Oke et al. 1995) on Keck. These observations cover an important fraction of the areal footprint of the SSA22 *Chandra* field (see Figure 1). In some observations (Keck LRIS, VLT VIMOS), we obtained flux calibrated spectra through

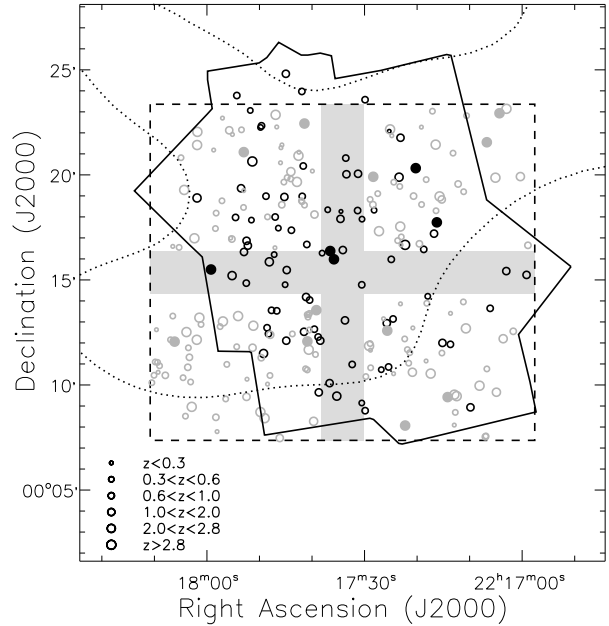


Figure 1. Positions of extragalactic sources in our sample. The black and gray circles are sources observed with Keck (DEIMOS and LRIS), and VLT VIMOS, respectively. The circles have been plotted with sizes that increase with redshift. The filled circles correspond to sources that potentially belong to the SSA22 protocluster ($3.06 \leq z \leq 3.12$). The dashed square indicates the area covered by the six VIMOS slit masks; the gray cross indicates the chips gaps. The polygon correspond to ensemble the area covered by the Keck slit masks. The dotted line is an isodensity contour marking where most of the optically selected LAEs at $z \sim 3$ reside (from Hayashino et al. 2004).

the use of response curves obtained from standard stars. In these cases, the spectra have been corrected by atmospheric extinction. Although Keck DEIMOS and VLT VIMOS lack an atmospheric dispersion compensator (ADC), we do not attempt atmospheric refraction corrections. This is because observations performed by these instruments are executed at small zenith angles with N-S oriented slits, and consequently, with negligible dispersion effects (see e.g., Filippenko 1982; Szokoly 2005; Sánchez-Janssen et al. 2014). When flux calibrated spectra are provided, we do not attempt to correct the spectra for slit losses (see e.g., Cassata et al. 2011). Therefore, in cases of flux calibration, the spectra are accurate to the 10–20% level.

2.1 VLT observations

The VIMOS observations were centered at the coordinates $22^{\text{h}}17^{\text{m}}34.20^{\text{s}}$, $0^{\circ}15'21.8''$ and span an area of $18' \times 16'$ (see Figure 1). These observations were performed in MOS (multi-object spectroscopy) mode using the HR BLUE grism. The wavelength coverage of 3700–6700 Å covers AGN emission lines (e.g., Ly α , C IV and C III) at $1.5 \lesssim z \lesssim 4$. The observations consisted of six slit masks, each with a total integration time of ~ 4 hrs for masks used in 2011 (masks 1–3; see Table 1 for details) and ~ 6 hrs for masks used in 2012 (masks 4–6; Table 1). The exposures times were

¹ See <http://astro.dur.ac.uk/~dma/SSA22/> for details on the *Chandra* Deep Protocluster Survey.

Table 1. Log of Keck and VLT spectroscopic observations.

MASK ID	INSTRUMENT	OBS. DATE	RA	DEC	P.A.	$N_{\text{new}}/N_{\text{rep}}$
SSA22a (Keck1)	DEIMOS	2009 Sep 16	22:17:42.74	00:16:44.7	-170.9	27/0
SSA22b (Keck2)	DEIMOS	2009 Sep 16	22:17:40.27	00:15:20.2	-133.5	27/5
SSA22c (Keck3)	DEIMOS	2009 Sep 17	22:17:17.05	00:16:32.8	-166.4	19/1
SSA22d (Keck4)	DEIMOS	2009 Sep 17	22:17:25.64	00:18:41.5	-128.0	16/1
SSA22e (Keck5)	LRIS	2009 Dec 15	22:17:33.53	00:18:36.8	+106.0	6/1
SSA22f (Keck6)	LRIS	2009 Dec 16	22:17:44.20	00:14:56.0	+99.1	7/2
2096 (VLT1)	VIMOS	2011 Jun 09	22:17:34.60	00:15:20.0	+90.0	98/0
2318 (VLT2)	VIMOS	2011 Sep 20	22:17:34.60	00:15:20.0	+90.0	100/0
2349 (VLT3)	VIMOS	2011 Sep 23	22:17:34.60	00:15:20.0	+90.0	53/6
2523 (VLT4)	VIMOS	2012 Jul 22	22:17:34.60	00:15:20.0	+90.0	11/64
2526 (VLT5)	VIMOS	2012 Aug 15	22:17:34.60	00:15:20.0	+90.0	10/54
2531 (VLT6)	VIMOS	2012 Aug 22	22:17:34.60	00:15:20.0	+90.0	5/27

Characteristics of the Keck and VLT slit masks observed in the SSA22 field, including the instruments, observation dates (UT), and mask center coordinates (J2000.0) and position angles. The number of new spectroscopic targets and those that have previously determined redshifts have been indicated as N_{new} and N_{rep} , respectively.

Table 2. Spectroscopically surveyed extragalactic sources.

OBJECT ID	RA ^a	DEC ^a	z	SDSS g^b	SUBARU R^b	UKIDSS K^b	S. TYPE ^c	MASKS ^d	QUALITY	CLASS ^e
VLT observations										
10031	334.27914	0.12557	0.6292	23.0	21.3	18.6	EllG	1,4	A	bri
10032	334.30383	0.13486	0.1000	20.4	21.1	20.2	EllG	1	B	bri
10034	334.49194	0.12968	0.1718	21.1	21.3	20.0	SFG	1,4	A	bri
10051	334.30301	0.14493	0.3839	22.7	21.1	18.8	EllG	3,5	A	bri
10077	334.45193	0.16735	0.1102	21.4	21.9	21.4	SpG	1,5	A	bri
10092	334.51294	0.16906	0.3034	21.8	21.5	19.5	SpG	1,4	A	bri
10110	334.42041	0.17862	0.3986	22.7	22.0	20.4	SpG	1,6	A	bri
10113	334.53757	0.18189	0.4213	23.0	21.8	20.3	SpG	1,6	A	bri
Keck observations										
006	334.24649	0.25400	1.1261	22.1	21.9	20.1	AGN	4	A	XR/bri
010	334.26257	0.25703	1.0252	...	24.9	20.2	AGN	4	B	XR
016	334.27536	0.22747	0.9070	...	24.7	21.7	SpG	4	A	XR
021	334.29099	0.14894	1.1123	...	25.3	21.5	SpG	3	B	XR
035p	334.30688	0.19892	0.7532	23.4	23.3	20.4	SpG	3	A	XR
038	334.31320	0.20006	1.7338	22.5	22.5	20.9	AGN	3	A	XR/bri
039	334.31378	0.31386	1.3997	22.1	21.7	20.5	AGN	3	A	XR/bri
043p	334.31766	0.29569	3.0980	...	24.5	...	AGN	3	A	XR/ $z \sim 3$

^aOptical positions in J2000.0 equatorial coordinates.

^bThe optical magnitudes presented in this Table come from the SDSS survey (e.g., Adelman-McCarthy et al. 2008), SSA22 photometric survey of Hayashino et al. (2004) (Subaru magnitudes) and the UKIDSS survey (e.g., Lawrence et al. 2007). The UKIDSS magnitudes have been transformed from Vega to AB magnitudes using $K(\text{AB})=K(\text{Vega})+1.9$ (from Hewett et al. 2006).

^cSpectral types are based on cross-correlation template that has minimum χ^2 (see details in §3). EllG \equiv elliptical galaxy; SpG \equiv spiral Galaxy; SFG \equiv starburst galaxy; LBG \equiv Lyman-break galaxy; AGN \equiv active galactic nuclei.

^dMasks where source presents A or B quality spectra.

^eTarget selection criteria classes. bri \equiv bright source ($R < 22.5$); XR \equiv X-ray source from the Lehmer et al. (2009b) catalog; $z \sim 3$ \equiv $z \sim 3$ LBG; $z \sim 4$ \equiv $z \sim 4$ LBG; Ste03 \equiv LBG from Steidel et al. (2003); LAE \equiv LAE from Hayashino et al. (2004).

Table 2 is presented in its entirety in the electronic version; an abbreviated version of the table is shown here for guidance as to its form and content.

selected in order to detect faint optical counterparts to limiting magnitudes of $R \approx 25$ for extragalactic sources with strong emission features and $R \approx 24$ for sources with moderate emission/absorption features. The spectra on each mask are reduced using the standard ESO VIMOS pipeline version 2.9.7.² This pipeline consist of routines from the VIMOS Interactive Pipeline and Graphical Interface (VIPGI; Scodreggio et al. 2005). The conditions were photometric, with $\lesssim 1''$ seeing and the resolving power of these observations is $\mathcal{R} \equiv \lambda/\Delta\lambda \sim 2300$. Each VIMOS mask had ~ 150 slits, of which $\sim 50\%$ provide spectra of sufficient quality for our template matching (see §3). The spectra obtained from the VIMOS pipeline contained some contamination of emission lines due to the spectral multiplexing and sky lines. The ranges where this contamination is present has been masked out from the spectra in order to perform cross-correlation template fits (see §3). The extracted VIMOS spectra were flux-calibrated using standard response curves³ obtained from repeated exposures of standard stars. The flux calibration has been further refined by comparing the brightness of stars observed in our survey (see Appendix A) with their SDSS photometry.

2.2 Keck observations

In 2009 September, we observed four slit masks (SSA22a-d) targeting X-ray sources in the SSA22 field with DEIMOS on the Keck II telescope. The DEIMOS masks typically each contained 75 targets and were observed for 1.5–2 hr, split into 20–30 min integrations; details of the observations are presented in Table 1. All observations used $1''.5$ wide slitlets and the 600 line mm^{-1} grating ($\lambda_{\text{blaze}} = 7500 \text{ \AA}$; $\mathcal{R} \sim 1600$). The conditions were photometric, with $0''.5$ seeing. The wavelength coverage of these observations was 4600–9700 \AA with a spectral resolution of $\approx 4 \text{ \AA}$. In 2009 December we observed two slit masks (SSA22e and f) targeting SSA22 X-ray sources using LRIS, a dual-beam spectrograph on the Keck I telescope. Each mask was observed for ~ 1 hr, split into three exposures. All observations used $1''.3$ wide slitlets, the 400 line mm^{-1} blue grism ($\lambda_{\text{blaze}} = 3400 \text{ \AA}$; $\mathcal{R} \sim 600$), and the 400 line mm^{-1} red grating ($\lambda_{\text{blaze}} = 8500 \text{ \AA}$; $\mathcal{R} \sim 700$). Slit mask SSA22e, observed the first night, used the 5600 \AA dichroic, while SSA22f, observed the following night, used the 6800 \AA dichroic. Conditions were clear for the LRIS observations. When LRIS spectra were observed in both the blue and the red grism, we obtained a wavelength coverage of 3500–10000 \AA with a spectral resolution of $\approx 10 \text{ \AA}$. The DEIMOS data were processed using a slightly modified version of the pipeline developed by the DEEP2 team at UC-Berkeley (Cooper et al. 2012; Newman et al. 2013), while the LRIS data reduction followed standard procedures.

Given that our targets are X-ray sources and high-redshifts galaxies primarily, in the next sections we focus our analysis mainly on the extragalactic sources. In Appendix A we present information related to stellar sources observed in the field.

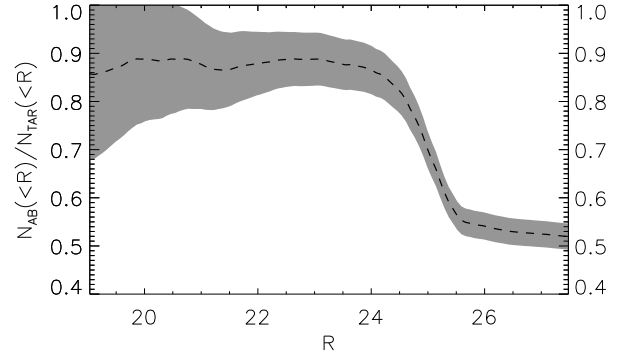


Figure 2. Ratio of the cumulative number A or B quality spectra to the cumulative number of total targets as a function of R magnitude. The shadow area are the $1\text{-}\sigma$ errors (Poisson errors are assumed).

3 SPECTRAL ANALYSIS

We targeted sources for spectroscopy based on three target selection criteria classes. The first category corresponds to sources in the *Chandra* X-ray catalog of the SSA22 field from Lehmer et al. (2009b). The second category includes bright sources with optical magnitudes $R < 22.5$.⁴ The third category corresponds to optically selected LBG and LAE candidates, further divided into four sub-categories: Steidel et al. (2003) $z \sim 3$ LBG candidates, new $z \sim 3$ or $z \sim 4$ LBG candidates (see §4.2 for details), and LAE candidates from Hayashino et al. (2004). The majority of Keck targets correspond to sources in the X-ray catalog of Lehmer et al. (2009b).

To determine redshifts and spectral types for our observed objects, we fit our spectra with several templates using the publicly available software SPECPRO (Masters & Capak 2011). The extragalactic templates used (see Appendix A for a description of the stellar templates) come from the VVDS (Le Fèvre et al. 2013) for Spiral (SpG), Elliptical (EllG), and Star-Forming Galaxies (SFG); Shapley et al. (2003) and Bielby et al. (2013) for LBGs in emission and absorption; Francis et al. (1991) for Seyfert galaxies; and Vanden Berk et al. (2001) for QSOs. For each spectrum, we select a cross-correlation template based on the minimum χ^2 . In general, almost every recognizable extragalactic spectrum will be well described by one of the templates. Therefore, based on the best-matched template we obtain redshifts and classify the spectra respectively as SpG, EllG, SFG, AGN (for QSO or Seyfert), or LBG.

In Table 2, we present basic information for our observed objects. This table summarizes the results of our source spectroscopy, including the quality of the derived spectroscopic redshift (Q). Quality flag $Q = A$ signifies an unambiguous redshift determination, typically relying on an asymmetric line profile indicating Ly α emission (cf., Stern et al. 2000), a confidently identified continuum break in the spectroscopy (e.g., a Lyman-break or D4000 break), and/or the identification of multiple emission/absorption

² <http://www.eso.org/sci/software/pipelines>

³ <http://www.eso.org/observing/dfo/quality/VIMOS/qc/response.html>

⁴ The R -magnitudes come from the Subaru photometric survey

Hayashino et al. (2004)

Table 3. The ratio of A/B spectra to the number of targeted sources.

class ^a	VLT obs. $N_{\text{AB}}/N_{\text{TAR}}$	Keck obs. $N_{\text{AB}}/N_{\text{TAR}}$	VLT & Keck obs. $N_{\text{AB}}/N_{\text{TAR}}$
Bright	218/246	38/41	245/274
X-ray	35/94	97/186	120/233
$z \sim 3$ LBG	38/140	2/2	39/141
$z \sim 4$ LBG	12/70	0/1	12/71
All LBG	52/254	6/11	57/262
All classes	277/561	102/200	367/714

^a Target selection criteria class.

N_{AB} is the number of A or B quality spectra and N_{TAR} is the total number of targeted sources.

features. Quality flag $Q = B$ signifies a less certain redshift determination, where the asymmetry of the emission line was ambiguous, the continuum break was of uncertain identification, and/or only a single emission feature was identified. We consider $Q = B$ spectroscopic redshifts to be likely correct; however, additional spectroscopy would be beneficial. Some of the sources have been observed multiple times. In the last column of Table 1, N_{new} is the number of previously unobserved sources on a given mask, and N_{rep} is the number of sources which were also observed on a previous mask. N_{new} and N_{rep} account for quality A and B obtained in this work, including both extragalactic sources and stars. For cases of spectral quality A or B, the redshift errors are conservatively expected to be $\Delta z \lesssim 0.0005(1+z)$, based on the spectral resolution combined with uncertainties in the wavelength calibration. These errors are verified by comparing the redshifts obtained for sources with good quality spectra in more than one mask. For cases where the extragalactic sources were observed in more than one slit, we also checked the reliability of the redshift determinations obtaining cases where $\Delta z < 0.0025(1+z)$. For $Q = A$ and $Q = B$ spectra the reliability is 98% (62 out of 63 cases) and 97% (28 out of 29 cases), respectively. In Figure 2 we plot the ratio of the cumulative number of A/B quality spectra to the total number of targeted slits ($N_{\text{AB}}/N_{\text{TAR}}$) as a function of magnitude in the R -band. This ratio is more or less constant at $\sim 90\%$ with increasing R , up to $R \sim 24$. As expected, for $R > 24$ $N_{\text{AB}}/N_{\text{TAR}}$ declines dramatically. Table 2 includes the target selection criteria class; many of the sources that were previously classified as bright and a few of the X-ray sources were found to be stars (see Appendix A for details of stellar spectra). The ratio of A/B spectra to the number of targeted sources ($N_{\text{AB}}/N_{\text{TAR}}$) of each target class is as follows (Poisson errors are assumed): 0.89 ± 0.06 for bright, 0.52 ± 0.05 for X-ray, 0.28 ± 0.04 for $z \sim 3$ LBGs, and 0.17 ± 0.05 for $z \sim 4$ LBGs (see Table 3 for details).

In Figures 3 and 4 we plot flux/counts as a function of wavelength for the VLT and Keck spectra of extragalactic sources respectively; identified absorption and emission lines of the best matched spectral template are indicated. The spectral classification for most sources was based on templates that match the source spectra for at least two noticeable absorption/emission features. The exceptions to this are the LBGs (see §4.2 for more details). In total we

have spectroscopically classified (with A/B quality) 164 extragalactic sources and 113 stars in the VLT observations, and 94 extragalactic sources and 8 stars in the Keck observations. In section 4.5, we describe in more detail the spectra of three sources that show peculiar spectral features. Discounting overlaps (matching radius $\leq 1''.3$) between the VLT and Keck observations, we have obtained reliable spectra for a total of 247 unique extragalactic sources and 120 unique Galactic stars. For sources observed by both the VLT and Keck observations, we found consistency in the wavelength range where the spectra overlapped.

4 RESULTS AND DISCUSSION

4.1 Comparison with Published Redshifts

We compare our redshifts with those from published spectroscopic surveys that include the SSA22 field. These surveys include the Garilli et al. (2008) VIMOS VLT Deep Survey (VVDS; Le Fèvre et al. 2005a), the LAE FOCAS Subaru surveys by Matsuda et al. (2005) and Yamada et al. (2012), and the Keck LBG survey by Steidel et al. (2003). We selected sources in those surveys that were within an area of $23' \times 23'$ centered on the VLT survey center. The selected area is large enough to cover the LBG fields SSA22a from Steidel et al. (2003) and the *Chandra* survey from the SSA22 field (Lehmer et al. 2009b). In the published surveys, we select sources with redshift quality similar to those of our surveys. In the case of the VVDS survey, we select only flags 3 and 4, which indicates a redshift reliability above 95%. Additionally in the Steidel et al. (2003) surveys, we selected only secure redshift identifications of optically selected LBG candidates with a strong emission feature (identified as a $\text{Ly}\alpha$ emission line) and/or cases of multiple absorption features. Therefore, the spectral quality of the selected sources in Steidel et al. (2003) is very similar to $Q = A$ or $Q = B$ spectra from this work (see §4.2). Finally, the LAE redshift identifications of Matsuda et al. (2005) and Yamada et al. (2012) correspond to cases of a high S/N emission feature often complemented with multiple absorption features. Therefore, the selected LAE redshift identifications are equivalent to $Q = A$ or $Q = B$ spectra from this work as well (see §4.2). Using this criterion, there are 494 source redshifts available in published catalogs, including 281 reliable redshifts from the VVDS survey, 100 sources from Steidel et al. (2003), and 113 sources from the LAE surveys. Note that we do not count sources that are repeated across the published surveys. For repeated sources (angular distance $< 1''.3$), we have taken the following arbitrary order of priority (from highest to lowest priority): the Steidel et al. (2003) LBG survey, the LAE survey of Yamada et al. (2012), the LAE survey of Matsuda et al. (2005), and then the VVDS survey.

The redshift distribution of our sample is compared with those available in the literature in Figure 5. The VVDS survey provides the majority of redshifts at $z \lesssim 1.0$, while the other surveys dominate the source redshift distribution at $z > 2.0$. By design, the LAE surveys are very concentrated on sources at $z \approx 3.0$ (see §4.3). Our spectroscopy included 41 sources that already had redshifts from the public surveys (matching radius $< 1''.3$). In these sources we do not find major differences between our redshifts and published

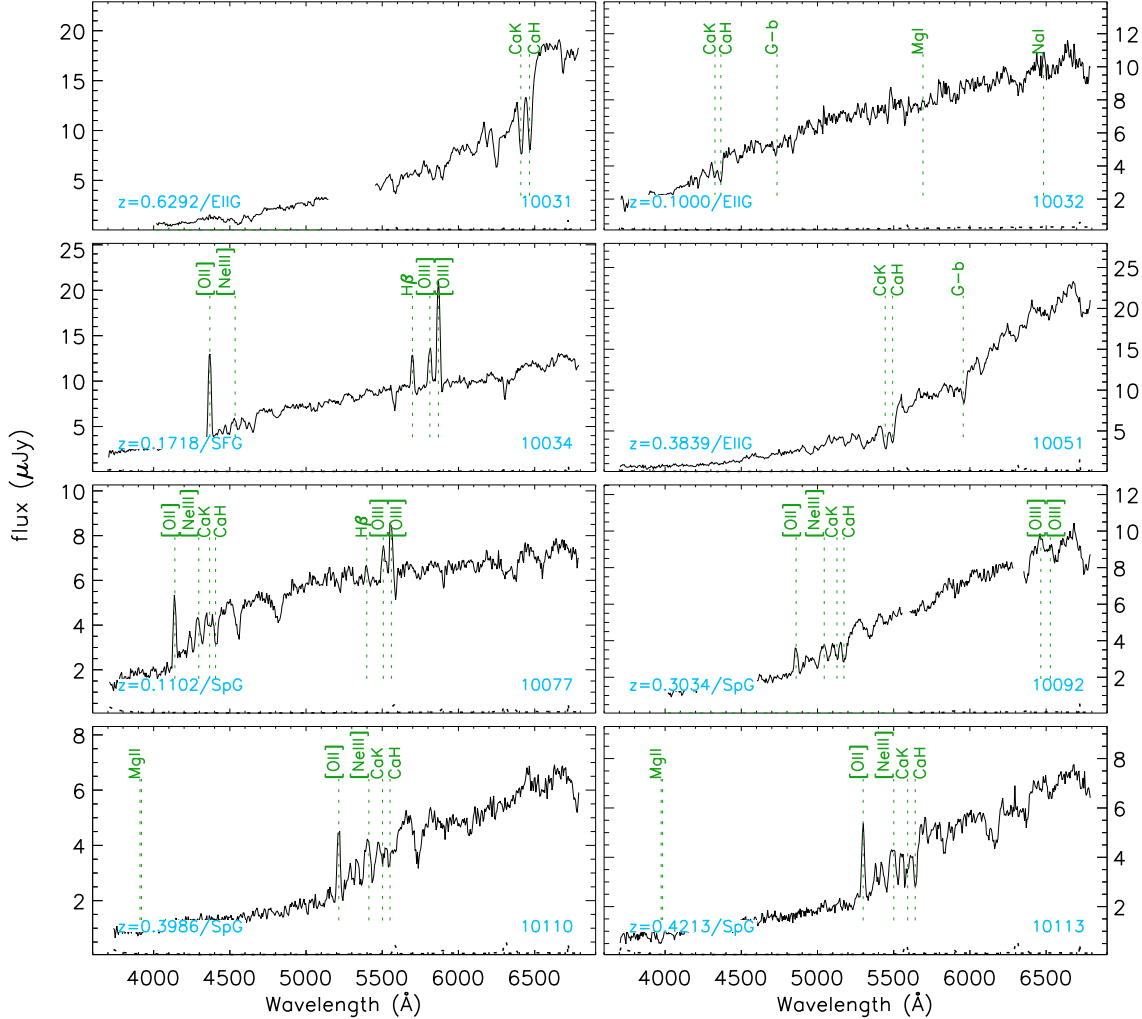


Figure 3. Sample VLT VIMOS spectra. In each figure key absorption and emission features of the corresponding template used to fit the spectrum are marked for reference. For display purposes only the first eight VIMOS spectra are shown. Please refer to the electronic version to see all the spectra.

redshifts ($\Delta z < 0.005(1+z)$). Therefore, we spectroscopically identified 206 (247 total minus 41 previously classified) new extragalactic sources, a $\approx 42\%$ increase in the number of reliable spectroscopic redshifts. Our major contribution comes in the redshift range between $1.0 \leq z \leq 2.0$ and $z \geq 3.4$, where we have increased the number of sources with redshifts by factors of 3.5 (from 12 to 42) and 13 (from 1 to 13), respectively. The sources at $1.0 \leq z \leq 2.0$ come mainly from the Keck observations, since DEIMOS and LRIS probe wavelengths up to $\approx 1\mu\text{m}$. The sources at $z \geq 3.4$ were obtained by targeting LBGs candidates at $z \sim 4$ with VLT-VIMOS (see §4.2).

4.2 Lyman-Break Galaxies

Our LBG template was used to fit $z > 2$ galaxies that have been optically classified either as LBGs or LAEs. The

majority of LBGs have been previously classified in four groups: $z \sim 3$ LBGs, $z \sim 4$ LBGs (from the photometric survey of Hayashino et al. 2004), optical LBGs candidates from Steidel et al. (2003), and optical LAEs candidates from Hayashino et al. (2004).

The criteria to select $z \sim 3$ LBGs was:

- (1) $22 \leq R \leq 25.5$
- (2) $U - V - 2(V - R) \geq 1.0$
- (3) $U - V \geq 1.0$
- (4) $V - R \leq 0.3$
- (5) $R - z \leq 0.2$

The criteria to select $z \sim 4$ LBGs was:

- (1) $U(\text{CFHTLS}) > 27.2$
- (2) $B - i - 2.3(i - z) \geq 1.9$
- (3) $V - i - 1.61(i - z) \geq 0.5$
- (4) $R - i \leq 1.2$
- (5) $B - i \geq 1.9$
- (6) $i - z \leq 0.15$
- (7) $i \leq 26.0$

Note that in the last expressions CFHTLS stands for Canada-France-Hawaii Telescope. With the exception of one

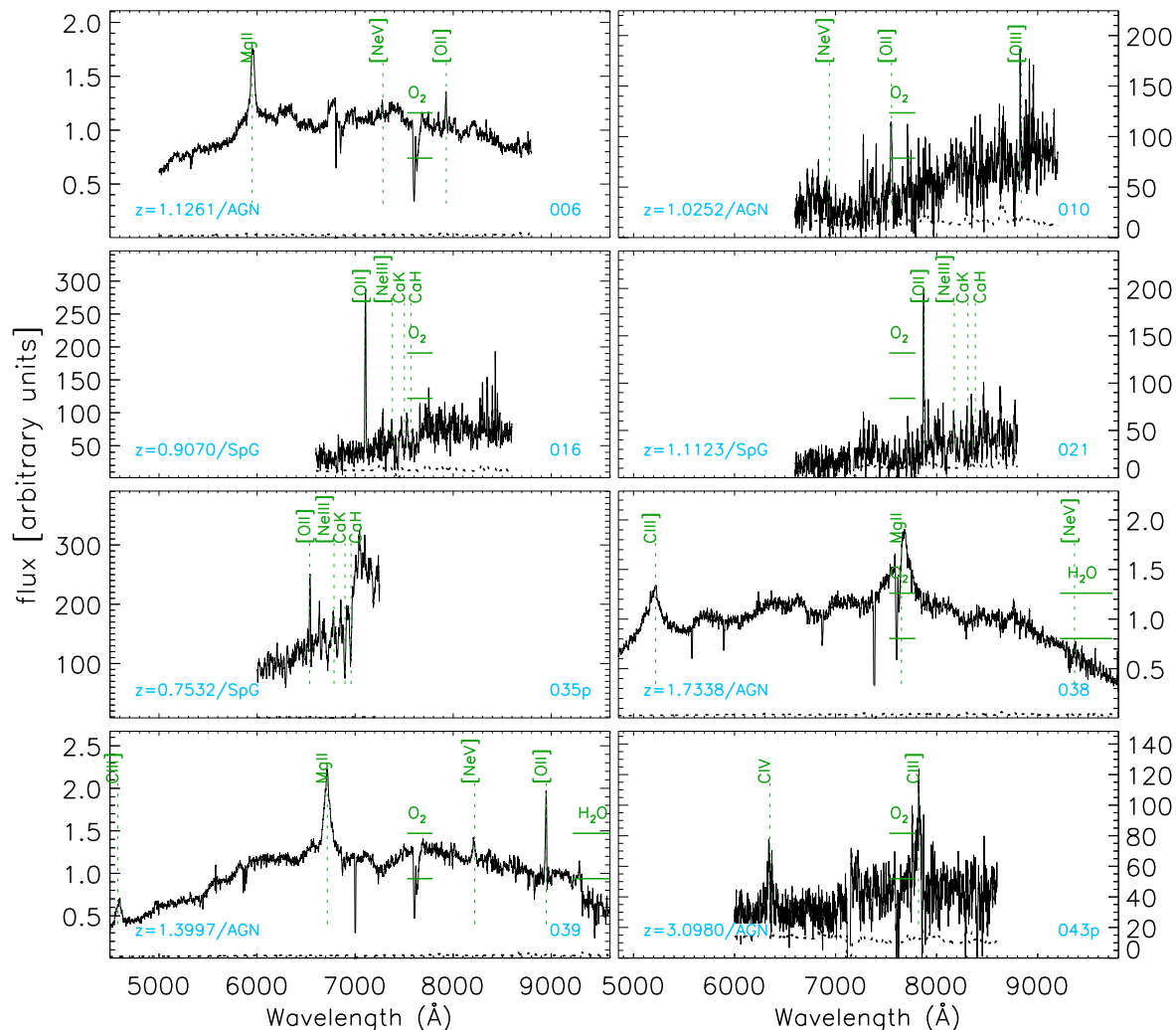


Figure 4. Sample Keck DEIMOS and LRIS spectra. In each figure key absorption and emission features of the corresponding template used to fit the spectrum are marked for reference. For display purposes only the first eight Keck spectra are shown. Please refer to the electronic version to see all the spectra.

source (VIMOS source 21164; see Figure 6 and Table 2), the LBGs show clear evidence of a single strong emission line, assumed to be Ly α . VIMOS source 21164 ($R = 23.7$) was the only case found with Ly α absorption. This feature was accompanied by at least three absorption lines, allowing a very reliable cross correlation match with our LBG absorption template (see Figure 6). Among the absorption lines observed the spectrum of source 21164 are: Si II λ 1260, O I+Si II λ 1303 and C II λ 1334. The VLT (Keck) observations showed evidence for high-redshift ($z > 2$) LBG spectral signatures in 43 (2) sources. Discounting overlaps with published redshifts, we found a total of 36 new sources with LBG spectral signatures (including LBGs and LAEs). Since the Keck observations exclusively targeted *Chandra* X-ray sources, all LBGs from Keck are X-ray emitters.

In the sample of LBG candidates at $z \sim 3$ and $z \sim 4$ we found eight cases in which the spectrum did not match the

typical characteristics of an LBG. Five out of the eight cases were stars (see Appendix A); the other three cases include an ELLG at $z = 0.023$ (10979), an SFG at $z = 0.345$ (11281), and an SpG at $z = 0.514$ (21493). As a test of possible contamination from low-redshift sources, we tried other templates to fit the LAE or LBG candidates. These alternative templates do not present improved fits over the LBG template. For example, the SFG and SpG templates confuses the strong LBG Ly α emission feature with [O II] λ 3727 in the redshift range $0.1 \lesssim z \lesssim 1.0$; however, we would expect to observe other features as well (e.g. [Ne III] λ 3864, H β λ 4861, [O III] λ 5007) that are not present. Only the spectra of VLT sources 11281 and 21493 exhibit these features. Indeed, the LBG template does not present any important emission features besides Ly α λ 1216, though it does have absorption features such as Si II λ 1263, O I λ 1304, C II λ 1335 and Si IV λ 1397. With the exception of three spectra (21164, 21186, and 31167; see

Table 4. Distribution of $z \sim 3$ and $z \sim 4$ LBG candidates in two magnitude bins.

Sources	With Spectroscopic z	$z \sim 3$		$z \sim 4$	
		$R < 25$	$R \geq 25$	$R < 25$	$R \geq 25$
Published and not in this work ^a	Yes	37	17	2	1
Published and in this work ^b	Yes	3	4	0	0
This work only ^c	Yes	14	18	6	6
Not $Q=A, B$ targets with redshifts ^d	Yes	5	2	1	0
Not $Q=A, B$ targets with no redshift ^e	No	31	64	15	43
No information	No	80	181	58	363

The area where the sources were selected correspond to a $23' \times 23'$ square centered on the coordinates $22^{\text{h}}17^{\text{m}}34.20^{\text{s}}, 0^{\circ}15'21.8''$ (J2000).

^a Sources with published redshifts and with no $Q = A$ or B redshifts from this work.

^b Sources with published redshifts and with $Q = A$ or B redshifts from this work.

^c Sources with $Q = A$ or B redshifts from this work only.

^d Targets from this work that did not result in $Q=A$ or B spectra and with redshifts from published surveys.

^e Targets from this work that did not result in $Q=A$ or B spectra and with no redshifts from published surveys.

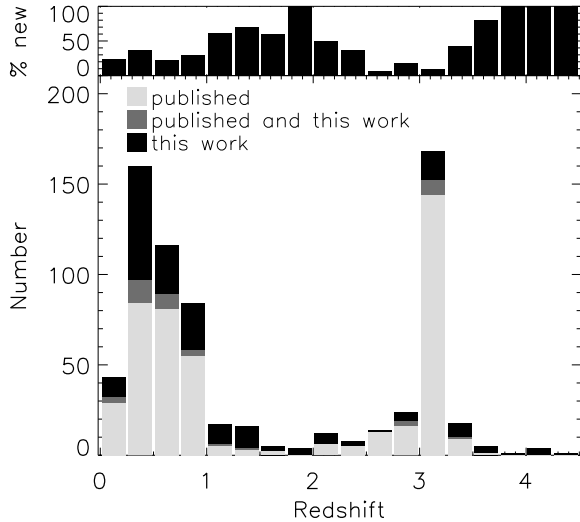


Figure 5. Redshift distribution of sources in the SSA22 field. These sources have been selected inside a $23' \times 23'$ square centered on the coordinates $22^{\text{h}}17^{\text{m}}34.20^{\text{s}}, 0^{\circ}15'21.8''$ (J2000). The dark and light gray histograms represent sources collected by published redshift surveys with and without overlap with our surveys. The black histogram represents sources with new redshifts from our survey. The upper panel indicates the redshift distribution of the fraction of new sources coming from our surveys.

Figure 3), there are no clear cases of absorption features in our LBG spectra. In general, our observations are unable to probe the continuum of LBGs. This is expected given that the majority of the optically selected LBGs have $R > 24$. Indeed, S/N in the spectral continua of successfully identified LBGs is low ($\langle S/N \rangle_{\text{cont}} \approx 7$).

Within the area selected to concentrate this study (see §4.1), we check the completeness of the LBG selection by comparing the total number of LBG candidates to the number that have spectroscopic redshifts (see Figures 7 and 8). The total number of $z \sim 3$ sources with redshifts is 93, with 32 being new redshifts from our survey (see Table 4). The total number of $z \sim 4$ sources with redshifts is 15, with 12 coming from our survey (see Table 4). Figures 7 and 8, and

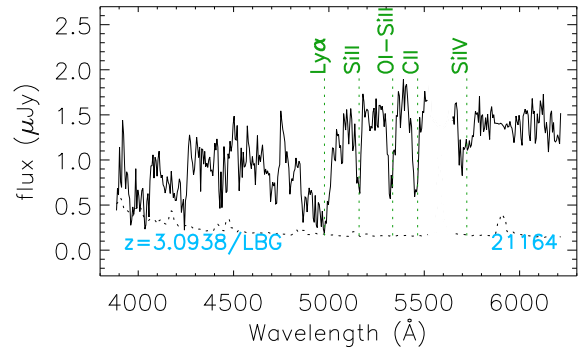


Figure 6. LBG absorption spectrum of VLT source 21164. Some absorption lines of the LBG absorption template have been shown for reference.

Table 4 show that our survey is far from complete, particularly for sources at $z \sim 4$. If we include all the spectroscopic information available (including this work), $\approx 33\%$ and $\approx 14\%$ of the $R < 25$ and $R \geq 25$ sources have spectroscopic redshifts for $z \sim 3$ candidates, respectively. Additionally, $\approx 10\%$ and $\approx 2\%$ of the $R < 25$ and $R \geq 25$ sources have spectroscopic redshifts for $z \sim 4$ candidates, respectively. Thus, $N_{\text{AB}}/N_{\text{TAR}}$ in our LBG spectroscopic redshift survey was 0.32 ± 0.08 and 0.25 ± 0.05 for the $R < 25$ and $R \geq 25$ $z \sim 3$ sources, and 0.27 ± 0.11 and 0.12 ± 0.05 for the $R < 25$ and $R > 25$ $z \sim 4$ sources (see details in Figures 7 and 8, and Table 4), respectively. These numbers suggest that we are only detecting LBGs with strong Ly α emission; in general, our observations are not deep enough to probe the continua of these sources.

Similar to this work, Cassata et al. (2015) observed high redshift sources with VLT-VIMOS. Their sample included sources with $i' < 25$ and photometric redshifts $z_{\text{phot}} = 2-6$. For sources with spectral VVDS flags 3 or 4 (equivalent to $Q = A/B$ in our survey, see §4), Cassata et al. (2015) found $N_{\text{AB}}/N_{\text{TAR}}$ fractions of 0.43 ± 0.02 and 0.40 ± 0.03 for $2.7 < z_{\text{phot}} < 3.5$ and $3.5 < z_{\text{phot}} < 4.5$, respectively. These fractions are higher than our values of $N_{\text{AB}}/N_{\text{TAR}}$ for $z \sim 3$ and $z \sim 4$ LBGs with $R < 25$. However, these differences are expected given that the Cassata et al. (2015) VIMOS

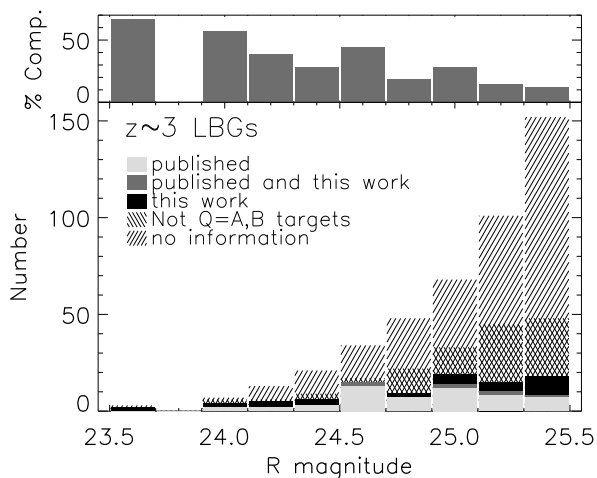


Figure 7. Magnitude distribution of $z \sim 3$ optically selected LBG candidates in the SSA22 field. These sources have been selected inside a $23' \times 23'$ square region centered on the coordinates $22^{\text{h}}17^{\text{m}}34.20^{\text{s}}$, $0^{\circ}15'21.8''$ (J2000). The dark and light gray histograms represent sources collected from published redshift surveys with and without overlap with our sample. The black histograms represent new redshifts from our observations. The line-filled histograms with upper-left orientation represent targeted sources from our survey without recognizable spectra. The line-filled histograms with upper-right orientation represent sources without spectroscopic redshift information. The upper panel indicates the completeness distribution of the sample counting sources from our survey and published surveys.

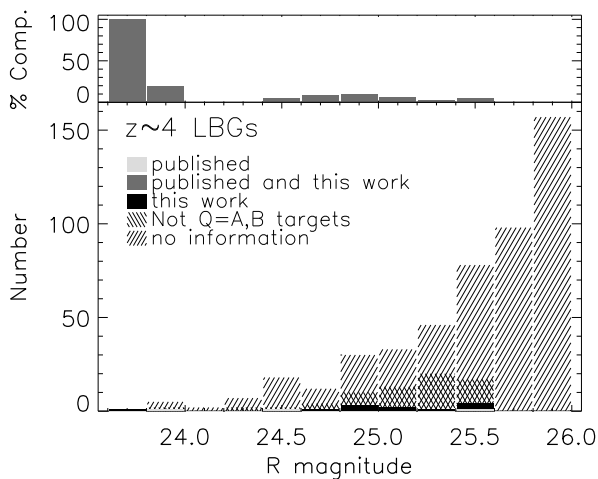


Figure 8. Magnitude distribution of $z \sim 4$ optically selected LBG candidates in the SSA22 field. For details about this figure refer to the caption of Figure 7

masks were observed twice, including one 14 hr exposure using a blue filter (LRBLUE) and one 14 hr exposure using a red filter (LRRED). As we discussed earlier in this section, our LBG targets were mainly concentrated in our VLT observations and not in the Keck observations. Therefore, the Cassata et al. (2015) exposures are typically a factor of

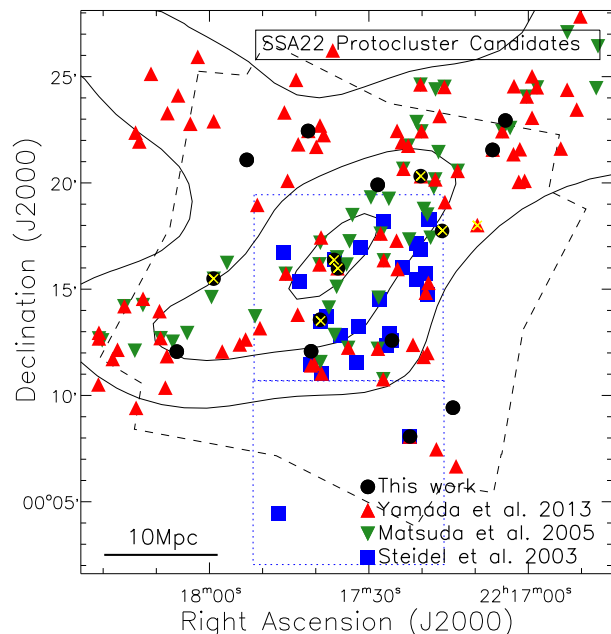


Figure 9. Positions of surveyed sources likely belonging to the SSA22 protocluster ($3.06 \leq z \leq 3.12$). Filled circles, triangles, inverted triangles and squares correspond to sources in our survey, the LAE survey of Yamada et al. (2012), the LAE survey of Matsuda et al. (2005), and the LBG survey of Steidel et al. (2003) respectively. The dashed polygon indicates the area of the *Chandra* SSA22 point source catalog (Lehmer et al. 2009b). The two dotted squares indicate the SSA22a and SSA22b LBG Steidel et al. (2003) surveys, respectively. The contours show source isodensity levels of optically selected LAE candidates at $z \sim 3$ from Hayashino et al. (2004). The X symbols indicate sources with detected X-ray emission. The bottom left shows the angular extent of a transverse comoving distance of 10 Mpc at $z = 3.091$.

~ 3 times deeper and cover a broader wavelength range than our VLT observations of SSA22 LBGs, which explains the differences in $N_{\text{AB}}/N_{\text{TAR}}$.

4.3 New protocluster candidates

We identify new SSA22 protocluster candidates as sources with redshifts $3.06 \leq z \leq 3.12$. This range of redshifts covers a comoving length of ≈ 56 Mpc. The chosen range more or less agrees with the expected extension of this protocluster, which covers a comoving area of approximately $60 \times 30 \text{ Mpc}^2$ (as shown in Hayashino et al. 2004 and Figure 9). Based on this criterion, we found 16 sources in our survey and 134 unique additional sources in published catalogs. We find eight overlapping sources between our observations and the public surveys and hence we report 8 new protocluster candidates (see Figure 9). Most of the protocluster candidates found in our sample (12 out of 16) are from the optically selected LBGs at $z \sim 3$ (see §4.2); the rest are two X-ray selected quasars and two LAE/X-ray AGNs (see §4.4). The SSA22 protocluster members from the published catalogs come from optically selected LBGs (27 sources from Steidel et al. 2003) and LAEs (107 sources

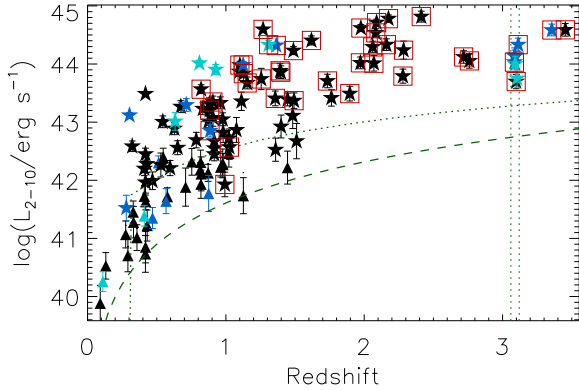


Figure 10. X-ray luminosity versus redshift. The 2–10 keV X-ray luminosities have been determined from the X-ray fluxes in Lehmer et al. (2009b) assuming power-law spectra (see §4.4). The filled stars and triangles indicate sources that have and have not been classified as AGN candidates (according to the selection criteria of §4.4). The black and light-blue sources have redshifts from this work and published data, respectively. Blue symbols indicate sources with redshifts from both our survey and published surveys. Sources that have AGN-type optical spectrum are marked with a square. The dashed curve indicates the sensitivity limit of the *Chandra* SSA22 field survey assuming a power-law spectra with $\Gamma = 1.8$ (Lehmer et al. 2009b). The dotted curve corresponds to the expected quasar sensitivity for a magnitude limit of $R = 25.5$. To obtain this curve, we assumed a power law optical-UV spectrum with $\alpha = -0.5$ (e.g., Vanden Berk et al. 2001) and transformations between the optical and X-ray bands following Marconi et al. (2004). The vertical dotted lines indicate the redshift range of the SSA22 protocluster.

from Matsuda et al. 2005; Yamada et al. 2012). The protocluster candidates from Steidel et al. (2003) are primarily from the SSA22a field, which contains the central region of the protocluster (see Figure 9). Our criteria to select $z \sim 3$ LBGs (see §4.2) are similar to those used by Steidel et al. (2003); a large fraction ($\approx 48\%$) of Steidel et al. (2003) sources are identified by our LBG selection scheme. In contrast, our $z \sim 3$ LBG selection criteria is almost independent of the LAE optical selection criteria of Hayashino et al. (2004). For example, for the LAEs with spectroscopic redshifts, only $\approx 14\%$ of the sources match our selection criteria for $z \sim 3$ LBGs. Additionally, the LAE selection criteria are focused on detecting sources in a narrower range of redshifts (at $z \approx 3$) than our $z \sim 3$ LBG selection criteria. Specifically, the average spectroscopic redshift of the LAEs is $\langle z \rangle = 3.08$ with a standard deviation of 0.02 compared to an average redshift $\langle z \rangle = 3.11$ with standard deviation of 0.21 for the $z \sim 3$ LBGs.

4.4 X-ray sources

The ~ 400 ks *Chandra* Deep Protocluster survey reaches sensitivities of $\sim 3 \times 10^{-16}$ erg cm $^{-2}$ s $^{-1}$ in the observed 2–8 keV X-ray band. The catalog of Lehmer et al. (2009b) consists of 297 X-ray point source detections. For the Keck observations we targeted X-ray sources by using counterpart positions from the optical/near-infrared observations

reported in Lehmer et al. (2009b), which are registered to the astrometric frame of the UKIRT Infrared Deep Sky Survey (UKIDSS; Lawrence et al. 2007) Deep Extragalactic Survey (DXS) of the SSA22 field. In cases where there is not clear *K*-band identifications, we sometimes simply put a slitlet on the X-ray position while for others we would target a nearby *K*-band source. In the case of the VLT observations we targeted the X-ray sources when their optical counterparts (from Lehmer et al. 2009b) were detected in the VIMOS pre-image. We associate a spectrum with an X-ray source if its angular distance to a X-ray counterpart is less than $(\sqrt{\Delta\theta^2 + 2})''$. The last expression corresponds to the sum of squares of $\Delta\theta$ (the X-ray positional error found in Table 2 of Lehmer et al. 2009b) and $\sqrt{2}$ which is an estimation of the expected positional error between optical sources and their X-ray counterpart.

The new spectroscopic classifications for X-ray sources and their respective X-ray IDs (from Table 2 of Lehmer et al. 2009b) is presented in Table 5 and the details of the columns are given below.

Column (1) gives IDs from Table 2 of Lehmer et al. (2009b).

Column (2) gives IDs in case the source belongs to our survey.

Column (3) gives the referred surveys where a source has been spectroscopically observed. 1≡this work; 2≡Steidel et al. (2003); 3≡Yamada et al. (2012); 4≡Matsuda et al. (2004); 5≡Le Fèvre et al. (2005b).

Columns (4) and (5) give optical positions in J2000.0 equatorial coordinates.

Column (6) gives angular distance (in $''$) between the X-ray source and the spectroscopically identified source.

Column (7) gives redshifts, either from our survey or published surveys in case the source is not in our survey.

Column (8) gives the Subaru AB *R*-band magnitudes from the SSA22 photometric survey of Hayashino et al. (2004).

Column (9) gives the monochromatic AB magnitude at rest-frame wavelength 2500 Å. These were computed by extrapolating the flux densities obtained from the optical magnitudes. Previous to the extrapolation, the flux densities obtained have been corrected for Galactic reddening.

Column (10) gives the logarithm of the monochromatic luminosity at rest-frame 3.6 μm (with units erg s $^{-1}$ Hz $^{-1}$). These values were computed from the flux densities at rest-frame wavelength 3.6 μm . The flux densities at rest-frame wavelength 3.6 μm have been obtained by interpolating a power-law fit between two Galactic reddening *Spitzer* corrected flux densities (observed at 3.6, 4.5, 5.8 and 8.0 μm). If the *Spitzer* observed bands do not cover the rest-frame wavelength 3.6 μm , the flux densities at rest-frame 3.6 μm are obtained from their closest wavelength observed flux densities assuming a power-law spectrum $f_\nu \propto \nu^\alpha$ with $\alpha = -1.0$ (e.g., Stern et al. 2005).

Column (11) gives the logarithm of the monochromatic luminosity at rest-frame 2500 Å (with units erg s $^{-1}$ Hz $^{-1}$).

Column (12) gives the logarithm of the monochromatic luminosity at rest-frame 2 keV (with units erg s $^{-1}$ Hz $^{-1}$) obtained from observed X-ray fluxes from Table 2 of Lehmer et al. (2009b) (see this section for more details).

Column (13) gives the difference between the logarithm of the monochromatic luminosity at rest-frame 2

Table 5. Spectral properties of extragalactic X-ray sources with redshifts.

XID (1)	ID (2)	REF. (3)	RA (4)	DEC (5)	$\Delta\theta$ (6)	z (7)	R (8)	AB_{2500} (9)	$\log L_{3.6\mu\text{m}}$ (10)	$\log L_{2500}$ (11)	$\log L_{2\text{keV}}$ (12)
4	...	5	334.24249	0.36628	1.0	0.9266	23.4	24.49	30.80	28.11	25.94±0.09
6	006	1	334.24615	0.25372	1.5	1.1261	21.9	21.79	...	29.36	25.87±0.13
7	10516	1	334.25137	0.33200	0.1	2.2845	21.2	20.71	31.58	30.36	26.28±0.15
8	...	5	334.25208	0.35658	1.1	0.6328	23.2	23.98	29.46	27.98	25.05±0.15
10	010	1	334.26251	0.25714	0.5	1.0252	24.9	25.80	29.96	27.68	24.61±0.29
11	20518	1	334.27042	0.16092	0.0	2.4122	26.9	25.75	...	28.39	26.85±0.09
16	016	1	334.27557	0.22722	1.2	0.9070	24.7	25.40	29.55	27.73	25.11±0.14
20	...	3	334.29001	0.30003	0.9	3.1050	24.5	25.03	30.12	28.86	25.79±0.21

The optical magnitudes used to obtain AB_{2500} , L_{2500} , α_{ox} , and $\log R_L$ come from the SDSS survey (e.g., Adelman-McCarthy et al. 2008), the SSA22 photometric survey of Hayashino et al. (2004) (Subaru magnitudes) and the UKIDSS survey (e.g., Lawrence et al. 2007). The flux densities at rest-frame 2500Å and 4400Å (from which we obtain AB_{2500} , L_{2500} , α_{ox} , and $\log R_L$) were obtained by interpolating a power-law fit between two Galactic reddening corrected flux densities obtained from optical magnitudes. If the observed optical flux densities wavelengths do not cover the rest-frame 2500Å/4400Å, the flux densities at rest-frame 2500Å/4400Å were obtained from the closest wavelength observed flux densities assuming a power-law spectrum $f_\nu \propto \nu^\alpha$ with $\alpha = -0.5$ (e.g., Vanden Berk et al. 2001). Table 5 is presented in its entirety in the electronic version; an abbreviated version of the table is shown here for guidance as to its form and content. See §4.4 for details on the columns and their associated units.

keV and the expected value from Steffen et al. (2006) (i.e., $\log L_{2\text{keV}} = 0.721 \log L_{2500} + 4.531$).

Column (14) gives the logarithm of the 2–10 keV band luminosity (with units erg s^{-1}) obtained from observed X-ray fluxes of Table 2 of Lehmer et al. (2009b) (see this section for more details).

Column (15) gives the optical-to-X-ray power-law slope $\alpha_{\text{ox}} = \log(f_{2\text{keV}}/f_{2500})/\log(\nu_{2\text{keV}}/\nu_{2500})$. Where $f_{2\text{keV}}$ and f_{2500} are the flux densities at rest-frame 2 keV and 2500Å, respectively.

Column (16) gives the logarithm of the radio-loudness parameter ($R_L = f_{5\text{GHz}}/f_{4400}$). Where f_{4400} is the flux densities at rest-frame 4400Å. The flux densities at rest-frame 5 GHz have been obtained using flux densities at 1.4 GHz obtained from the radio images of Chapman et al. (2003) assuming a power-law spectrum $f_\nu \propto \nu^\alpha$ with $\alpha = 0$.

Column (17) gives 1 if the source is an AGN candidate, 0 otherwise. This is based on our AGN selection criteria described in this section.

In the VLT observations, we found reliable redshifts for 35 X-ray sources. The Keck observations exclusively targeted the X-ray sources, and therefore the majority of this sample (97 out of 102) correspond to X-ray sources. After accounting for the 12 overlapping X-ray sources between the Keck and VLT surveys, in total we found 120 redshifts for X-ray sources, of which only 15 overlap with redshifts available from published catalogs and 11 are stars. Therefore, we found redshifts for 94 new extragalactic X-ray sources. Of the 109 extragalactic X-ray sources in our survey, 58 are classified as ELIGs or SpGs, 9 are SFGs, 3 are LBGs and 39 are AGNs. Prior to this work there were only 23 X-ray sources with published spectroscopic redshifts; with this work we increase this to a total of 128 (117 of which are extragalactic sources), an increase by a factor ≈ 5.6 . Note that Lehmer et al. (2009b) reports on 46 X-ray sources with redshifts, though many of these sources are unpublished and from VVDS sources with less secure redshifts than the ones used in this work. In Table 2 of Lehmer et al. (2009b) there

are 25 redshifts from the unpublished work of Chapman et al. (2009). Of these 25 sources, we obtained redshifts for 13 and in just 4/13 our redshift measurement matches the one provided in Table 2 of Lehmer et al. (2009b). All 13 overlapping sources have $Q = A$ spectra. Therefore, the Chapman et al. (2009) redshifts do not seem to be robust enough to be used in this work.

Using the redshifts of our survey and those from published catalogs, we obtain X-ray luminosities in the 2–10 keV band L_X , and monochromatic 2 keV luminosities ($L_{2\text{keV}}$) from the observed X-ray fluxes found in Table 2 of Lehmer et al. (2009b). The X-ray luminosities are estimated assuming a power-law spectrum ($L_\nu = C\nu^\alpha$; $\Gamma = 1 - \alpha$) with $\Gamma = 1.8$ (e.g., Page et al. 2005). By default the luminosities are obtained by extrapolating the observed hard-band (2–8 keV) fluxes. In cases where the sources were not detected in the hard-band (2–8 keV), the observed fluxes were obtained in either the soft-band (0.5–2 keV) or the full-band (0.5–8 keV).

We classify our X-ray sample as AGN candidates based on similar criteria to that adopted by Lehmer et al. (2012):

(i) *X-ray Luminosity*: for cases in which $L_X > 3 \times 10^{42} \text{ erg s}^{-1}$, we can reliably classify the source as an AGN (e.g., Bauer et al. 2004).

(ii) *X-ray Spectral Shape*: hard X-ray spectra are indicative of dominant and powerful X-ray AGN that are significantly obscured. We select such hard AGN candidates based on their hardness ratios, with a cut at an effective $\Gamma < 1$.

(iii) *X-ray-to-Optical Flux Ratio*: X-ray-to-optical flux ratios indicate X-ray emission which is significantly elevated compared to normal galaxies. We identify AGN candidates based on $\log(f_X/f_R) > 1.0$ where f_X is either in the HB, FB or SB.⁵

⁵ $\log(f_X/f_R)$ is obtained from $\log(f_{0.3-3.5}/f_V) = \log f_{0.3-3.5} + V/2.5 + 5.37$ (where $f_{0.3-3.5}$ is the 0.3–3.5 keV flux in $\text{erg cm}^{-2} \text{ s}^{-1}$; Maccacaro et al. 1988). Assuming $V - R = 0.22$ which is the expected value for a $\alpha = -0.5$ AGN spectra (e.g.,

(iv) *X-ray-to-Radio Luminosity Ratio*: X-ray emission, as measured by radio emission, is significantly higher than expected from pure star formation; i.e., $L_{0.5-8\text{keV}} > 5 \times 4 \times 10^{18} L_{1.4\text{GHz}}$, where $L_{1.4\text{GHz}}$ is the rest-frame 1.4 GHz monochromatic luminosity in units of W Hz^{-1} and $4 \times 10^{18} L_{1.4\text{GHz}}$ is the expected X-ray emission level that originates from starburst galaxies (e.g., Bauer et al. 2002; Ranalli et al. 2003; Mineo et al. 2014).⁶ The radio fluxes are obtained from the SSA22 VLA radio images of Chapman et al. (2003) with an assumed spectral index of $\alpha_r = 0$ (White et al. 1997); $L_{0.5-8\text{keV}}$ is obtained from L_X assuming a power-law spectra with $\Gamma = 1.8$.

(v) *Optical spectroscopy*: Based on our source classification for sources is in our spectroscopic survey. For the few cases that sources are not in our spectroscopic sample, we search for evidence of AGN features in the literature if applicable.

Our criteria indicate 84 (out of 117) of the X-ray extragalactic sources are AGNs. In our optical spectroscopy, only 39 out of 78 of the AGNs candidates were spectroscopically classified as AGNs. The lack of AGN features in the optical spectra in half of the X-ray AGNs is expected from AGN obscuration (e.g., Alexander et al. 2001; Barger et al. 2005). In Figure 10 we show the X-ray luminosity versus redshift for the X-ray sources. Note that the sensitivity limit of the SSA22 *Chandra* survey implies that every X-ray source above $z \gtrsim 1.5$ is an AGN.

We find 7 sources that potentially belong to the SSA22 protocluster ($3.06 < z < 3.12$). These sources have X-ray luminosities $L_{2-10} \gtrsim 5 \times 10^{43} \text{ erg s}^{-1}$ implying they are quasars⁷ with $L_{\text{bol}} \gtrsim 10^{45} \text{ erg s}^{-1}$ (e.g., Marconi et al. 2004). The SSA22 protocluster candidates with X-ray detections are marked with X symbols in Figure 9. In the work of Lehmer et al. (2009b) there are 9 reported X-ray sources at $3.06 \lesssim z \lesssim 3.12$; however, 3 of the 9 sources came from the unpublished work of Chapman et al. (2009). As mentioned earlier, we do not adopt Chapman et al. (2009) redshifts in this work. Of the seven X-ray protocluster candidates, five are from our spectroscopy (one new source found in our survey), and three show QSO signatures in their optical spectra. Our sample of X-ray protocluster candidates might not be complete. The missing sources could be missed targets or cases with fainter fluxes than the sensitivity limits of our survey. For example the X-ray source 120 in the Lehmer et al. catalog, has a photometric redshift within the range $3.06 \lesssim z \lesssim 3.12$ (Tamura et al. 2010). This source was targeted by our survey, but the resulting spectrum did not show any recognizable feature. Additionally, observations of this source at sub-millimeter wavelengths complemented by a hard photon index ($\Gamma = -0.3 \pm 0.6$) strongly indicate an obscured protocluster quasar (Tamura et al. 2010). From

Akiyama et al. 2000) and correcting $f_{0.3-3.5}$ to the observed flux f_X (either at 2–8 keV, 0.5–8 keV or 0.5–2 keV) assuming $\Gamma = 1.8$.
⁶ From Bauer et al. (2002) the following relationship is obtained: $\log L_{0.5-8\text{keV}} = 0.935 \log L_{1.4\text{GHz}} + 20.141$ (where $L_{0.5-8\text{keV}}$ is in erg s^{-1} and $L_{1.4\text{GHz}}$ is in W Hz^{-1}) and therefore in the range of radio luminosities where this relationship is valid (i.e. $19 \lesssim \log L_{1.4\text{GHz}} \lesssim 24$) $L_X \sim 4 \times 10^{18} L_{1.4\text{GHz}}$; ($L_X \approx 0.68 \times L_{0.5-8\text{keV}}$ for a power-law spectrum with $\Gamma = 1.8$).

⁷ Quasars are defined here as AGNs with with bolometric luminosities $L_{\text{bol}} \gtrsim 10^{44} \text{ erg s}^{-1}$.

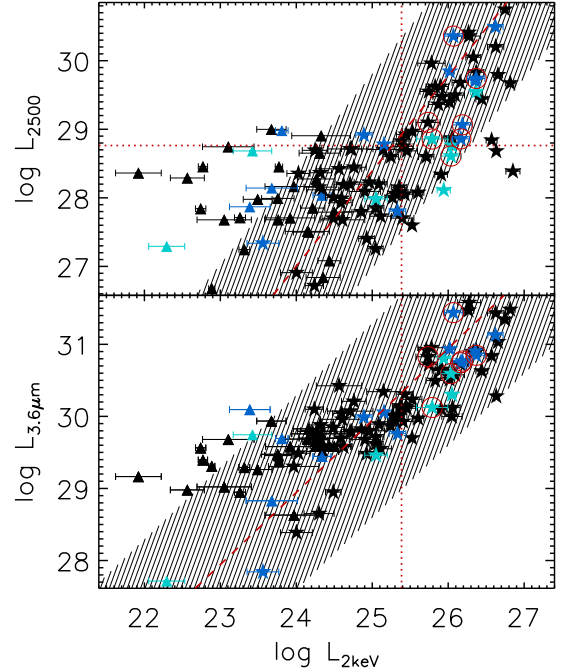


Figure 11. Infrared $3.6 \mu\text{m}$ (lower panel) and ultraviolet 2500 \AA (upper panel) luminosity versus 2 keV luminosity for X-ray sources in the *Chandra* Deep Protocluster survey. Monochromatic luminosities used here have units of $\text{erg s}^{-1} \text{ Hz}^{-1}$. Circles indicate sources that potentially belong to the SSA22 protocluster ($3.06 \leq z \leq 3.12$). The dashed lines in the lower and upper panel are the linear relations estimated from Steffen et al. (2006) and Richards et al. (2006) and the shadow regions are their respective $2\text{-}\sigma$ confidence limits. The dotted vertical lines in the lower and upper panels are the sensitivity limits of the SSA22 *Chandra* survey at $z = 3.091$ assuming a power-law spectrum with $\Gamma = 1.8$. The dotted horizontal line in the upper panel is the $R = 25.5$ sensitivity limit at $z = 3.091$ assuming a power-law optical-UV spectrum with $\alpha = -0.5$ (e.g., Vanden Berk et al. 2001). Symbols and colors of the sources are described in the caption of Figure 10.

the photometric redshifts of Kubo et al. (2013), we also expect to find additional X-ray protocluster members. In the mentioned work, it is found that there are 19 X-ray sources within $2.6 < z < 3.6$. In contrast, we found 11 sources in this redshift range, and therefore, more X-ray protocluster members with reasonable optical magnitudes for spectroscopy may exist.

To check additional properties of the X-ray sample, we plot the 2 keV luminosity versus the $3.6 \mu\text{m}$ luminosity and the 2 keV luminosity versus the 2500 \AA luminosity in Figure 11. With the exception of some outliers, our AGN candidates satisfy the $L_{2500} - L_{2\text{keV}}$ relation of Steffen et al. (2006). The $L_{3.6\mu\text{m}}$ to $L_{2\text{keV}}$ ratio of X-ray AGN candidates seem to match the expected values when compared to the Richards et al. (2006) SEDs (see lower panel Figure 11).

In this work we obtained the radio loudness parameter by extrapolating optical and radio flux densities. The

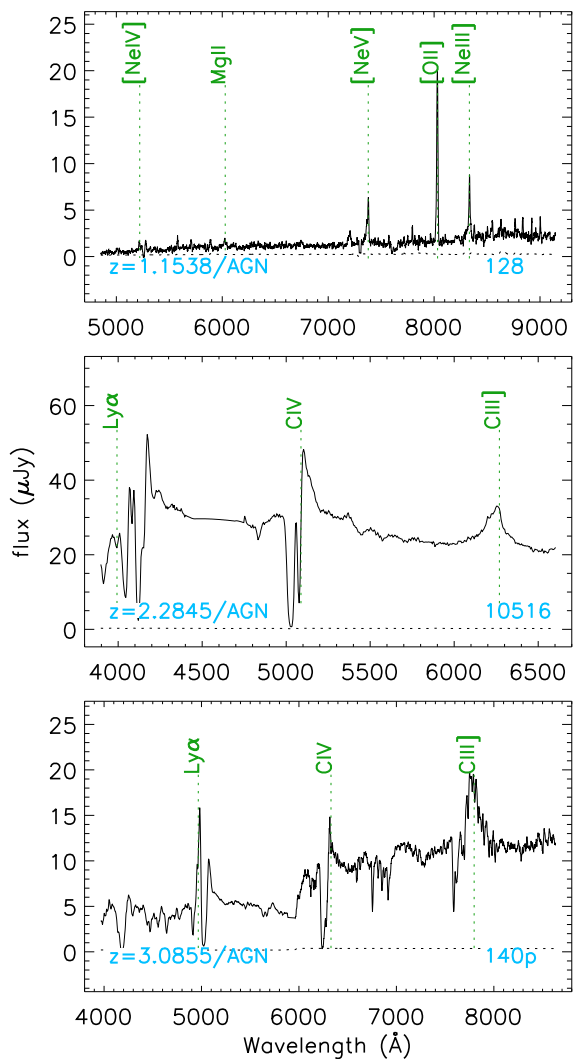


Figure 12. Three peculiar spectra in the SSA22 field. In each figure key emission lines of the AGN templates have been marked for reference.

radio flux densities were sensitive enough⁸ to properly discriminate between radio-loud (those with $\log R_L > 1.0$) and radio-quiet (those with $\log R_L \leq 1.0$) AGNs for a fraction of our sample. In our X-ray extragalactic sample 12 sources (nine AGNs) have radio detections with four of them corresponding to radio-loud AGN with moderate radio loudness parameters ($1.2 \lesssim \log R_L \lesssim 1.6$). Additionally, at least 23 (four protocluster candidates) out of the 75 AGNs that do not have radio detection cannot be excluded (with $\log R_L$ upper limits ≥ 1.5) from being radio-loud (see Table 5).

4.5 Peculiar spectra in the SSA22 Field

In this section we describe three X-ray sources with peculiar spectrum.

⁸ The limiting 1.4 GHz sensitivity is $60 \mu\text{Jy}$ (5σ ; Chapman et al. 2003).

4.5.1 X 128: A Ne-Rich Type-2 AGN at $z = 1.154$

X 128 is a moderate-redshift type-2 AGN showing an interesting set of emission lines at $z = 1.154$, with line ratios atypical of composite obscured AGN spectra (see Figure 12). Specifically, several ionization states of neon are particularly strong, including [Ne IV] $\lambda 2424$, [Ne III] $\lambda 3343$, [Ne V] $\lambda 3346$, [Ne V] $\lambda 3426$, [Ne III] $\lambda 3869$, and [Ne III] $\lambda 3968$. In radio galaxy spectra, typically [Ne IV] $\lambda 2424$ is observed with comparable strength to C II] $\lambda 2326$ (e.g., McCarthy 1993; Stern et al. 1999), whereas here the [Ne IV] line appears at least $\gtrsim 10\times$ the C II] line strength. The observed lines are not unprecedented, however; for instance, these ionization states are all evident in *Hubble Space Telescope* Imaging Spectrograph (STIS) observations of the “hot spot” in the inner narrow-line region of the well-studied Seyfert 2 galaxy NGC 1068 (Kraemer et al. 1998; Kraemer & Crenshaw 2000). In that source, high S/N spectra, including several dozen emission lines from the UV through the optical, are modeled as coming from multiple photoionized gas components.

4.5.2 BAL quasars

In this work we found two BAL quasar spectra: VIMOS 10516 at $z = 2.285$ and LRIS 140p at $z = 3.086$ (see Figure 12). Both sources present Ly α $\lambda 1216$, C IV $\lambda 1549$ and C III] $\lambda 1909$ emission lines. These BAL quasars show C IV blue-shifted absorption with projected line-of-sight Doppler broadenings $\sim -5500 \text{ km s}^{-1}$ and $\sim -5000 \text{ km s}^{-1}$ for 10516 and 140p, respectively. These sources as expected present moderate-to-weak X-ray emission with respect to normal quasars (e.g., Gallagher et al. 2006; Gibson et al. 2009; Saez et al. 2012) with $\Delta \log L_{2\text{keV}} = -0.15$ and -0.35 for 10516 and 140p, respectively; where $\Delta \log L_{2\text{keV}}$ is the difference between $\log L_{2\text{keV}}$ and its expected value from the $L_{2500} - L_{2\text{keV}}$ relation of Steffen et al. (2006).

5 SUMMARY AND FUTURE WORK

In this paper we present a survey of extragalactic sources in the SSA22 field obtained using multi-object spectrographs on the VLT and Keck telescopes. We quantify redshifts for new LBGs in the redshift range of the SSA22 protocluster and X-ray sources in the *Chandra* Deep Protocluster Survey with the goals of finding new protocluster members and complementing previous studies performed in this field. The main results can be summarized as follows:

- (i) By template matching high quality VIMOS, DEIMOS, and LRIS spectra we have successfully identified redshifts for 247 extragalactic sources and 120 Galactic stars. Discounting matches with sources that have redshift identifications from published catalogs, we found redshifts for a total of 206 new extragalactic sources.
- (ii) We have substantially increased the number of sources with known redshifts in the redshift range between $1.0 \leq z \leq 2.0$ and $z \geq 3.4$, by factors of 3.5 and 13, respectively.
- (iii) By targeting LAE and LBG candidates, we have successfully identified redshifts for 36 new sources at $z > 2$ with Ly α spectral features. All but one source has strong Ly α

emission line; the exception (VLT 21164) has Ly α absorption.

(iv) We have identified 8 new SSA22 protocluster candidates ($3.06 \leq z \leq 3.12$), one of which is an X-ray detected quasar.

(v) We have increased the number of X-ray sources with reliable redshifts from 23 to 128, leaving the Lehmer et al. (2009b) catalog now $\approx 43\%$ complete.

(vi) Using a variety of multiwavelength criteria, we identified 84 out of the 128 X-ray sources in the SSA22 field as AGNs, with 7 AGNs protocluster candidates (one new from this work; $3.06 \leq z \leq 3.12$). These candidates correspond to quasars with bolometric luminosities $L_{\text{bol}} \gtrsim 10^{45}$ erg s $^{-1}$.

The spectroscopic survey performed in this work is far from complete. There is still an important fraction of X-ray sources without any spectral identification ($\approx 57\%$). Additionally, there are 184 optically identified $R < 25$ LBGs candidates without reliable redshifts. The level of completeness of LBGs at $z \sim 3$ and $z \sim 4$ with $R < 25$ is $\approx 33\%$ and $\approx 10\%$, respectively (see §4.2). Since most optically selected LBGs have $R > 24$, in general, our observations are neither probing the continuum nor the absorption spectra of LBGs. More and deeper spectral surveys are needed both to find a more complete sample of the SSA22 protocluster and to fully exploit the ~ 400 ks *Chandra* observation available in this field.

ACKNOWLEDGEMENTS

We would like to thank Ezequiel Treister and the anonymous referee for helpful discussions regarding the interpretations of our results. We would also like to thank Scott Chapman for providing radio images of the SSA22 field. CS acknowledges support from CONICYT-Chile (FONDECYT 3120198, Becas Chile 74140006, and the Anillo ACT1101). FEB acknowledges support from CONICYT-Chile (Basal-CATA PFB-06/2007, FONDECYT 1141218, gemini-conicyt 32120003, "EMBIGGEN" Anillo ACT1101), and Project IC120009 "Millennium Institute of Astrophysics (MAS)" funded by the Iniciativa Científica Milenio del Ministerio de Economía, Fomento y Turismo. The work of DS was carried out at Jet Propulsion Laboratory, California Institute of Technology, under a contract with NASA. JEG thanks the Royal Society.

Based on observations made with ESO Telescopes at the Paranal Observatory under programme IDs 085.A-0616 and 089.A-0405. Some of the data presented herein were obtained at the W.M. Keck Observatory, which is operated as a scientific partnership among the California Institute of Technology, the University of California and the National Aeronautics and Space Administration. The Observatory was made possible by the generous financial support of the W.M. Keck Foundation. The authors wish to recognize and acknowledge the very significant cultural role and reverence that the summit of Mauna Kea has always had within the indigenous Hawaiian community. We are most fortunate to have the opportunity to conduct observations from this mountain.

REFERENCES

- Adelman-McCarthy, J. K., et al. 2008, *ApJS*, 175, 297
Akiyama, M., et al. 2000, *ApJ*, 532, 700
Alexander, D. M., Brandt, W. N., Hornschemeier, A. E., Garmire, G. P., Schneider, D. P., Bauer, F. E., & Griffiths, R. E. 2001, *AJ*, 122, 2156
Barger, A. J., Cowie, L. L., Mushotzky, R. F., Yang, Y., Wang, W.-H., Steffen, A. T., & Capak, P. 2005, *AJ*, 129, 578
Bauer, F. E., Alexander, D. M., Brandt, W. N., Hornschemeier, A. E., Vignali, C., Garmire, G. P., & Schneider, D. P. 2002, *AJ*, 124, 2351
Bauer, F. E., Alexander, D. M., Brandt, W. N., Schneider, D. P., Treister, E., Hornschemeier, A. E., & Garmire, G. P. 2004, *AJ*, 128, 2048
Bielby, R., et al. 2013, *MNRAS*, 430, 425
Cassata, P., et al. 2011, *A&A*, 525, A143
—, 2015, *A&A*, 573, A24
Chapman, S. C., Lewis, G. F., Scott, D., Richards, E., Borys, C., Steidel, C. C., Adelberger, K. L., & Shapley, A. E. 2001, *ApJL*, 548, L17
Chapman, S. C., Scott, D., Windhorst, R. A., Frayer, D. T., Borys, C., Lewis, G. F., & Ivison, R. J. 2004, *ApJ*, 606, 85
Chapman, S. C., et al. 2003, *ApJ*, 585, 57
Cooper, M. C., Newman, J. A., Davis, M., Finkbeiner, D. P., & Gerke, B. F. 2012, *spec2d: DEEP2 DEIMOS Spectral Pipeline*, astrophysics Source Code Library
Digby-North, J. A., et al. 2010, *MNRAS*, 407, 846
Faber, S. M., et al. 2003, in *Society of Photo-Optical Instrumentation Engineers (SPIE) Conference Series*, Vol. 4841, *Instrument Design and Performance for Optical/Infrared Ground-based Telescopes*, ed. M. Iye & A. F. M. Moorwood, 1657–1669
Filippenko, A. V. 1982, *PASP*, 94, 715
Francis, P. J., Hewett, P. C., Foltz, C. B., Chaffee, F. H., Weymann, R. J., & Morris, S. L. 1991, *ApJ*, 373, 465
Gallagher, S. C., Brandt, W. N., Chartas, G., Priddey, R., Garmire, G. P., & Sambruna, R. M. 2006, *ApJ*, 644, 709
Garilli, B., et al. 2008, *A&A*, 486, 683
Geach, J. E., et al. 2005, *MNRAS*, 363, 1398
Gibson, R. R., et al. 2009, *ApJ*, 692, 758
Governato, F., Baugh, C. M., Frenk, C. S., Cole, S., Lacey, C. G., Quinn, T., & Stadel, J. 1998, *Nature*, 392, 359
Hayashino, T., et al. 2004, *AJ*, 128, 2073
Hewett, P. C., Warren, S. J., Leggett, S. K., & Hodgkin, S. T. 2006, *MNRAS*, 367, 454
Kraemer, S. B., & Crenshaw, D. M. 2000, *ApJ*, 532, 256
Kraemer, S. B., Ruiz, J. R., & Crenshaw, D. M. 1998, *ApJ*, 508, 232
Kubo, M., et al. 2013, *ApJ*, 778, 170
Lawrence, A., et al. 2007, *MNRAS*, 379, 1599
Le Fèvre, O., et al. 2003, in *Society of Photo-Optical Instrumentation Engineers (SPIE) Conference Series*, Vol. 4841, *Instrument Design and Performance for Optical/Infrared Ground-based Telescopes*, ed. M. Iye & A. F. M. Moorwood, 1670–1681
Le Fèvre, O., et al. 2005a, *A&A*, 439, 845
—, 2005b, *A&A*, 439, 877
—, 2013, *A&A*, 559, A14
Lehmer, B. D., et al. 2009a, *ApJ*, 691, 687

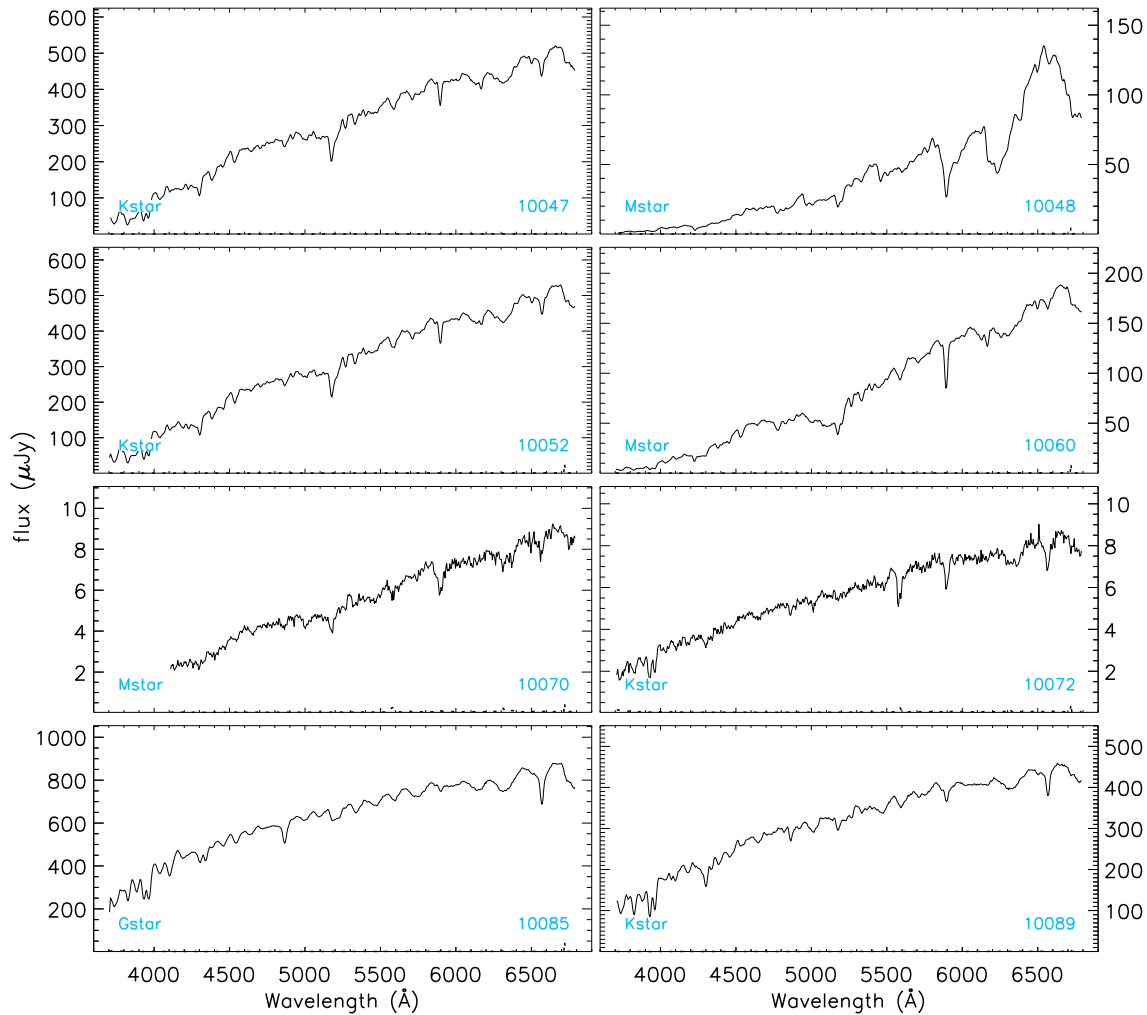


Figure A.1. VIMOS stellar spectra. For display purposes only the first eight VIMOS spectra are shown. Please refer to the electronic version to see all the spectra.

- . 2009b, MNRAS, 400, 299
- . 2012, ApJ, 752, 46
- . 2013, ApJ, 765, 87
- Maccararo, T., Gioia, I. M., Wolter, A., Zamorani, G., & Stocke, J. T. 1988, ApJ, 326, 680
- Marconi, A., Risaliti, G., Gilli, R., Hunt, L. K., Maiolino, R., & Salvati, M. 2004, MNRAS, 351, 169
- Martini, P., Sivakoff, G. R., & Mulchaey, J. S. 2009, ApJ, 701, 66
- Martini, P., et al. 2013, ApJ, 768, 1
- Masters, D., & Capak, P. 2011, PASP, 123, 638
- Matsuda, Y., et al. 2004, AJ, 128, 569
- . 2005, ApJL, 634, L125
- . 2011, MNRAS, 410, L13
- McCarthy, P. J. 1993, ARA&A, 31, 639
- Mineo, S., Gilfanov, M., Lehmer, B. D., Morrison, G. E., & Sunyaev, R. 2014, MNRAS, 437, 1698
- Morrison, R., & McCammon, D. 1983, ApJ, 270, 119
- Nestor, D. B., Shapley, A. E., Steidel, C. C., & Siana, B. 2011, ApJ, 736, 18
- Newman, J. A., et al. 2013, ApJS, 208, 5
- Oke, J. B., et al. 1995, PASP, 107, 375
- Page, K. L., Reeves, J. N., O'Brien, P. T., & Turner, M. J. L. 2005, MNRAS, 364, 195
- Pickles, A. J. 1998, PASP, 110, 863
- Ranalli, P., Comastri, A., & Setti, G. 2003, A&A, 399, 39
- Richards, G. T., et al. 2006, ApJS, 166, 470
- Saez, C., Brandt, W. N., Gallagher, S. C., Bauer, F. E., & Garmire, G. P. 2012, ApJ, 759, 42
- Sánchez-Janssen, R., Mieske, S., Selman, F., Bristow, P., Hammersley, P., Hilker, M., Rejkuba, M., & Wolff, B. 2014, A&A, 566, A2
- Scodreggio, M., et al. 2005, PASP, 117, 1284
- Shapley, A. E., Steidel, C. C., Pettini, M., & Adelberger, K. L. 2003, ApJ, 588, 65
- Steffen, A. T., Strateva, I., Brandt, W. N., Alexander,

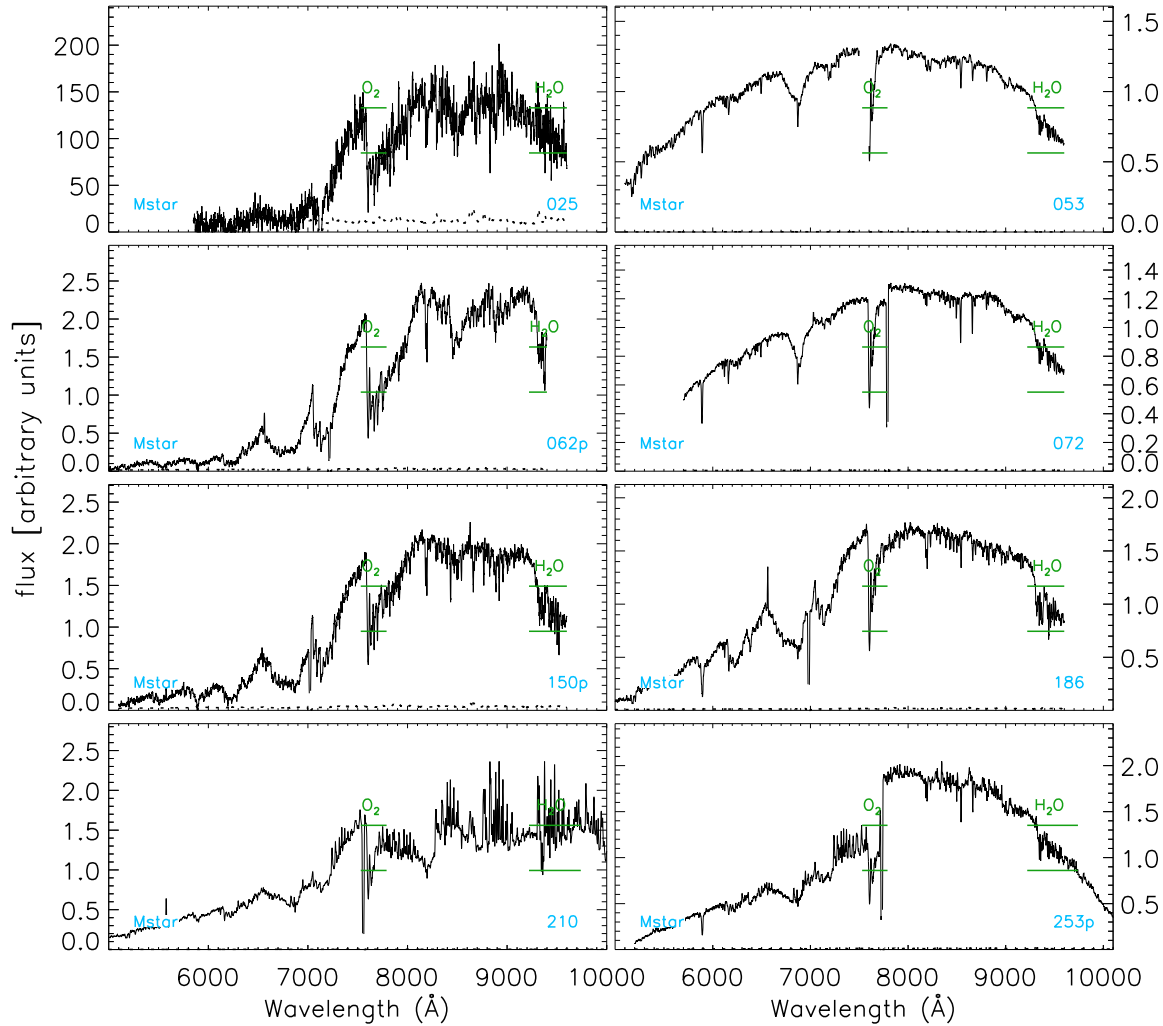


Figure A.2. DEIMOS and LRIS stellar spectra.

D. M., Koekemoer, A. M., Lehmer, B. D., Schneider, D. P., & Vignali, C. 2006, *AJ*, 131, 2826
 Steidel, C. C., Adelberger, K. L., Dickinson, M., Giavalisco, M., Pettini, M., & Kellogg, M. 1998, *ApJ*, 492, 428
 Steidel, C. C., Adelberger, K. L., Shapley, A. E., Pettini, M., Dickinson, M., & Giavalisco, M. 2000, *ApJ*, 532, 170
 —. 2003, *ApJ*, 592, 728
 Stern, D., Bunker, A., Spinrad, H., & Dey, A. 2000, *ApJ*, 537, 73
 Stern, D., Dey, A., Spinrad, H., Maxfield, L., Dickinson, M., Schlegel, D., & González, R. A. 1999, *AJ*, 117, 1122
 Stern, D., et al. 2005, *ApJ*, 631, 163
 Szokoly, G. P. 2005, *A&A*, 443, 703
 Tamura, Y., et al. 2009, *Nature*, 459, 61
 —. 2010, *ApJ*, 724, 1270
 —. 2013, *MNRAS*, 430, 2768
 Uchimoto, Y. K., et al. 2012, *ApJ*, 750, 116
 Ueda, Y., Akiyama, M., Ohta, K., & Miyaji, T. 2003, *ApJ*, 598, 886

Vanden Berk, D. E., et al. 2001, *AJ*, 122, 549
 Webb, T. M. A., Yamada, T., Huang, J.-S., Ashby, M. L. N., Matsuda, Y., Egami, E., Gonzalez, M., & Hayashimo, T. 2009, *ApJ*, 692, 1561
 White, R. L., Becker, R. H., Helfand, D. J., & Gregg, M. D. 1997, *ApJ*, 475, 479
 Yamada, T., Matsuda, Y., Kousai, K., Hayashino, T., Morimoto, N., & Umemura, M. 2012, *ApJ*, 751, 29

APPENDIX A: SPECTRA OF STARS IN THE SSA22 FIELD

As for extragalactic sources, Galactic stars were recognized by cross correlating template spectra with the data using the SPECPRO tool. The templates used (from Pickles 1998) allow us to get a reliable stellar classification based on main-sequence classes (A, F, G, K, and M stars). To classify stars we choose the template with minimum χ^2 . We found 113

Table A.1. Spectroscopically surveyed Galactic stars.

OBJECT ID	RA ^a	DEC ^a	SDSS g^b	SUBARU R^b	UKIDSS K^b	S. TYPE ^c	MASKS ^d	QUALITY	CLASS ^e
VLT observations									
10047	334.49319	0.14679	18.3	18.3	17.4	Kstar	1	A	bri
10048	334.52917	0.14442	20.9	19.4	17.2	Mstar	1,4	A	bri
10052	334.53781	0.14977	18.2	18.2	17.3	Kstar	1,4	A	bri
10060	334.52075	0.15687	20.0	18.9	17.8	Mstar	1,4	A	bri
10070	334.27811	0.16194	22.5	22.0	21.7	Mstar	1,4	B	bri
10072	334.35138	0.16143	22.3	22.0	22.1	Kstar	1,4	B	bri
10085	334.43250	0.17121	17.4	18.4	17.6	Gstar	1,3	A	bri
10089	334.33994	0.17206	18.1	18.6	18.0	Kstar	1	A	bri
Keck observations									
025	334.29446	0.18511	...	24.8	21.9	Mstar	3	A	XR
053	334.32986	0.24122	17.6	18.4	16.1	Mstar	3	A	XR/bri
062p	334.33701	0.17625	24.0	22.8	19.1	Mstar	2	A	...
072	334.34821	0.24539	21.2	20.0	18.9	Mstar	3	A	XR/bri
150p	334.41080	0.26592	24.6	23.0	20.4	Mstar	1	A	...
186	334.43619	0.29689	22.8	21.2	19.4	Mstar	2	A	XR/bri
210	334.44656	0.28000	17.4	18.5	14.2	Mstar	1	B	XR/bri
253p	334.47568	0.37325	21.0	19.6	18.1	Mstar	1	A	bri

^aOptical positions in J2000.0 equatorial coordinates.

^bThe optical magnitudes presented in this Table come from the SDSS survey (e.g., Adelman-McCarthy et al. 2008), SSA22 photometric survey of Hayashino et al. (2004) (Subaru magnitudes) and the UKIDSS survey (e.g., Lawrence et al. 2007). The UKIDSS magnitudes have been transformed from Vega to AB magnitudes using $K(AB)=K(Vega)+1.9$ (from Hewett et al. 2006).

^c Based on the cross-correlation star template that has minimum χ^2 .

^d Masks where source presents A or B quality spectra.

^e Target selection criteria classes. bri \equiv bright source ($R < 22.5$); XR \equiv X-ray source from the Lehmer et al. (2009b) catalog; $z\sim 3 \equiv z \sim 3$ LBG; $z\sim 4 \equiv z \sim 4$ LBG; Ste03 \equiv LBG from Steidel et al. (2003); LAE \equiv LAE from Hayashino et al. (2004).

Table A.1 is presented in its entirety in the electronic version; an abbreviated version of the table is shown here for guidance as to its form and content.

stars in the VLT observations (see Table A.1 and Figure A.1) and 8 stars in the Keck observations (see Table A.1 and Figure A.2). There is one star which was observed by both VLT and Keck, corresponding to 20644 (VLT) and 186 (Keck), such that we have surveyed a total of 120 Galactic stars. The majority are K and M stars (110/120) but we also find a few G and F stars (10/120).